Chapter 2
Methods to Determine Electrical Conductance of Single-Molecule Junctions

Ryo Yamada

Abstract In this chapter, three major experimental methods, i.e., a break junction (BJ) method, an electromigration (EM) method, and an ultrahigh-vacuum low-temperature scanning tunneling microscopy (UHV-LT-STM), to measure electrical properties of single-molecule junctions are explained with some remarkable example of studies. The BJ method is the most widely used technique and explained including statistical analytical methods to analyze data. Studies of molecular switch and temperature dependence are shown as examples of studies based on statistical analysis as well as examples of static current-voltage measurements with external field modulations. Techniques related to the BJ method such as distance modulation and electromechanical response measurements are also introduced. Although the EM method can suffer from several problems, it is still useful to measure electrical gate effects and in the preparation of nanoscale gap electrodes. A novel application of the EM method to create in-plane nano-holes that would open a new application field of the single-molecule measurement techniques is shown. The UHV-LT-STM is capable of forming single-molecule junctions on single-crystal surfaces and manipulating molecules on the surface that enables researchers to study single-molecule junctions under controlled and well-defined structures and environments.

Keywords Break junction • Electromigration • Scanning tunneling microscope • Statistical analysis • Conductance histogram • Two-dimensional histogram • Cross-correlation analysis • Distance modulation

2.1 Introduction

One of the great challenges in single-molecule electronics is the preparation of single-molecule junctions. In the early stages of experimental studies, metal contacts were deposited on top of monolayers prepared on metal surfaces by Langmuir-Blodgett and self-assembly techniques to investigate the charge transport through monolayers [1]. Other techniques including nano-pore technique [2],

R. Yamada (✉)
Graduate School of Engineering Science, Osaka University, Osaka, Japan
e-mail: yamada@molectronics.jp

M. Kiguchi (ed.), *Single-Molecule Electronics*, DOI 10.1007/978-981-10-0724-8_2

metal-nanoparticle contact [3–5], and cross wire contact [6] were developed. Although interesting characteristics of the single-molecule and monolayer junctions were reported, these techniques suffered low yield of working device and reproducibility. The poor reproducibility is attributed not only to the difficulty of experimental procedure itself but also to the nature of single-molecule junctions that have a wide variety of structures and flexibility.

A mechanical break junction method enabled researchers to obtain a large number of experimental results on the electrical conductance of the single-molecule junctions and to discuss results on both the statistics and the detailed static measurements on a single-molecule junction [7–10]. In this technique, a single-molecule junction is formed during the breaking of metal electrodes with molecules adsorbed on them by mechanical actuation mechanisms such as a scanning probe microscope and specially designed devices. Actuating mechanisms allow the broken electrodes to be reconnected so that measurements can be repeated. This technique enables researchers to conduct measurements on a large number of single-molecule junctions that make statistical analysis of the observed conductance possible in various environments such as vacuum, air, and solutions and at different temperatures. This technique can also be used to sustain a single-molecule junction to measure detailed current-voltage measurements and apply other important measurement techniques introduced in Chap. 3. The ability to tune the distance between two electrodes also used to control conformations of the junction mechanically.

In this chapter, techniques and the data analysis method used for the break junction methods are explained followed by brief introductions of other important measurement techniques, i.e., an electromigration technique and a scanning tunneling microscope, to fabricate single-molecule junctions. Summaries for other measurement techniques can be found in review articles [11–14].

2.2 Mechanical Break Junction Method

2.2.1 Principle and Instruments for the Break Junction Method

In the mechanical break junction (BJ) technique, a contact between two metal electrodes is broken by a precise mechanical control of a distance between the electrodes [7–10]. The BJ is conducted either scanning tunneling microscope (SMT-BJ) [15] and 3-point bending machines to break a metal contact prepared on an elastic substrate (mechanically controllable break junction (CBJ)) [16]. In this section, instruments and remarkable results on these techniques are explained.

2.2.1.1 Scanning Tunneling Microscope-Break Junction (STM-BJ)

In the STM-BJ, the STM tip is brought into contact with the substrate and the current during the retracting process is recorded. Figure 2.1a shows the relation between the current transient and structure of the junction during the breaking process. Initially, the electrical current decreases continuously following Ohm's law as the junction is stretched. When the dimension of the contact is as small as an atomic scale, stepwise decrease of the current is observed at the integer multiples of the quantum conductance $G_0 = 2e^2/h$. The exponential decay of the current is observed due to the tunneling transport after breaking the atomic contact of the electrodes (a dashed curve in Fig. 2.1a). When the molecule is adsorbed on the electrodes or existed in surrounding medium, conductance plateaus at conductance values below 1 G_0 are occasionally observed due to the formation of the single-molecule junction (a black curve in Fig. 2.1a). The single-molecule junction is broken by the further retraction of the STM tip. The break junction process can be repeated by making the STM tip contacted to the substrate repeatedly. The so-called current-distance or Z spectroscopy function implemented to most of commercial STM can be used to conduct the STM-BJ measurement.

The conductance of the single-molecule junction is determined based on the conductance histogram created from hundreds to thousands of the current transient curves (Fig. 2.1b). To create the conductance histogram, the number of data points measured at a certain range of conductance (bin-width of the histogram) is counted in a conductance transient curve. A conductance plateau enhances the count of the data points around the conductance value around it and a peak is formed in the conductance histogram. The current transients showing without any plateaus are sometimes removed to make the peak clearer.

Figure 2.2 shows conductance transient curves and conductance histograms obtained for 4,4′ bipyridine using gold electrodes. The conductance steps above 1 G_0 showing the formation of a gold atomic contact are evident in the conductance

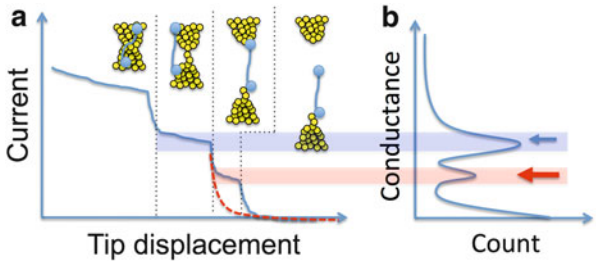

Fig. 2.1 (**a**) Scheme of a current transient observed during the retraction of the STM tip. Inset schematics show structures of the junction corresponding to the current steps. A *dashed smooth curve* shows the current decay without molecules. (**b**) A conductance histogram corresponding to the current transient shown in (*a*). The peaks indicated by *small* and *large arrows* correspond to the conductance of an atomic point contact, i.e., 1 G_0 for gold, and single-molecule junction, respectively

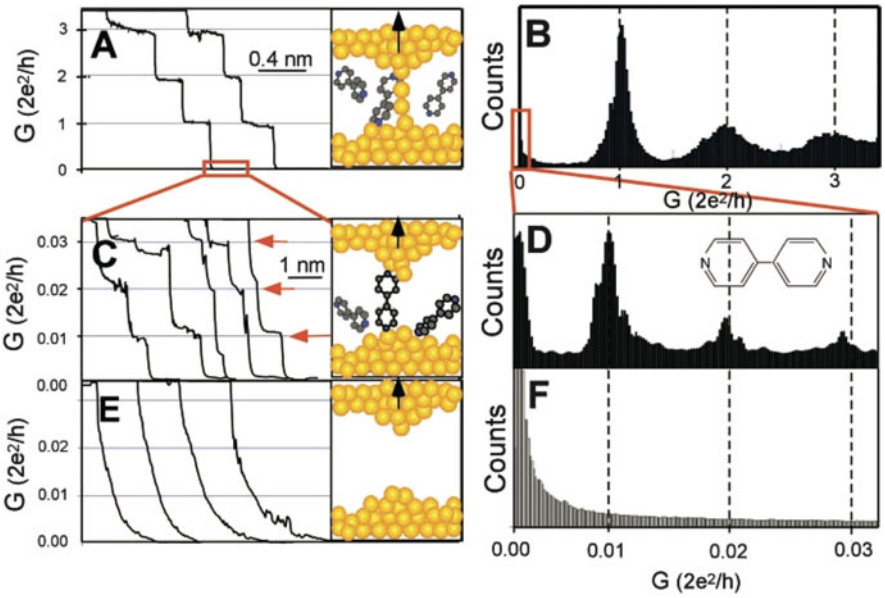

Fig. 2.2 (**a**) Conductance transient curves and (**b**) corresponding conductance histogram above 1 G_0 region measured by STM-BJ method using gold electrodes. (**c**), (**d**) represent conductance transient curves and corresponding conductance histogram below 1 G_0 region with the presence of 4,4′-bipyridine, respectively, whereas (**e**), (**f**) show them without any molecules [15]

transient curve (Fig. 2.2a) and histogram (Fig. 2.2b). The conductance transient curves pose additional plateaus below 1 G_0 with the presence of molecules as shown in Fig. 2.2c, and corresponding peak is found in the conductance histogram (Fig. 2.2d), whereas no plateaus are found without the presence of molecules (Fig. 2.2e, f). The conductance histogram shows multiple peaks at the integer multiples of the fundamental conductance of 0.01 G_0. The second and third peaks are attributed to two and three molecule junctions in parallel and considered as a strong evidence of the formation of a single-molecule junction at the fundamental conductance peak.

The detailed analysis of the conductance histogram sometimes reveals multiple sets of peaks [17–19]. Figure 2.3 shows conductance transient curves and histograms observed for Au/nonane-dithiol/Au junctions. The conductance plateaus are observed at different conductance ranges. The conductance histogram shows multiple peaks that can be assigned to three fundamental conductance values, indicated as L1, M1, H1, and their multiples. By comparing theoretical models, these peaks are attributed to the junction structures with different contact geometry as shown in Fig. 2.3e. The H1 and M1 correspond to the molecule junction in which the contact is formed at a bridge and an atop site, respectively. The L1 peak is assigned to the structure with bending in alkyl chain.

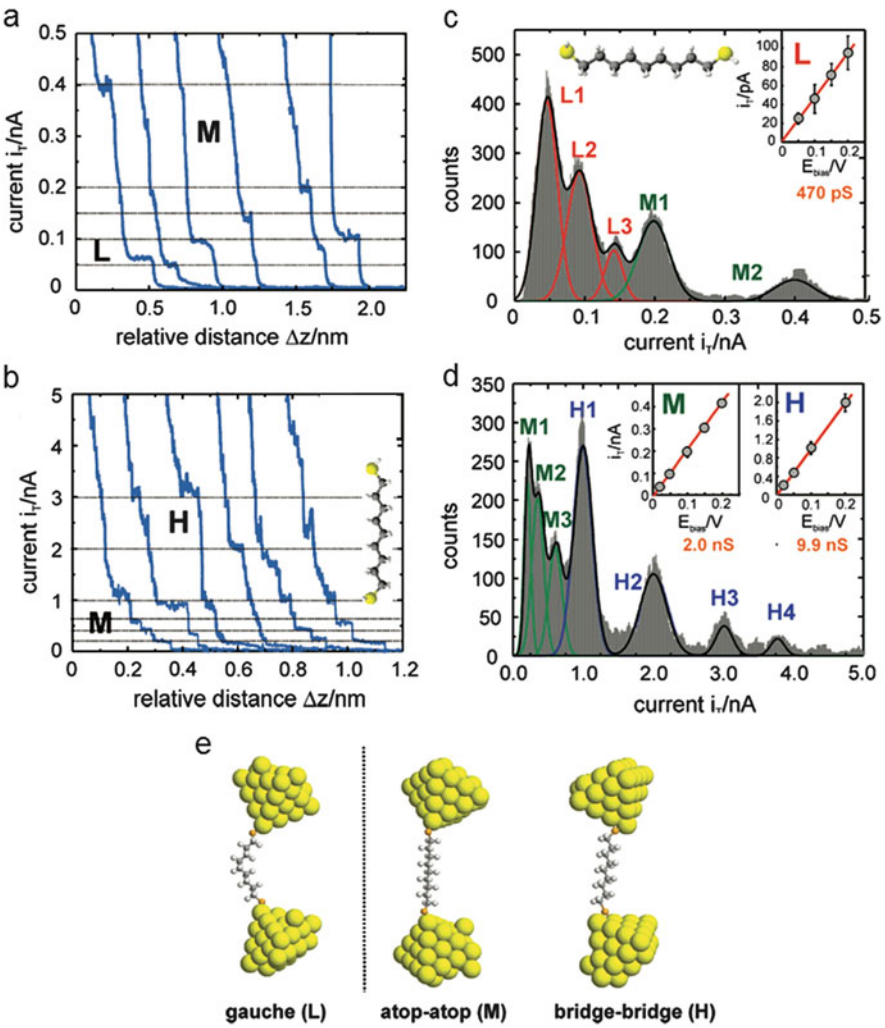

Fig. 2.3 Current transient curves observed low (**a**) and high (**b**) conductance regions and corresponding histograms (**c**, **d**). **e** Proposed models showing H, M and L conductance values [19]

The statistical method using the BJ method provided a way to quantify the single-molecule conductance and is now considered as the most standard method. Based on this technique, the charge transport mechanisms in the single-molecule junction such as length dependence [15, 20, 21], twisting between adjoining π-orbitals [22], anchoring chemistry [23, 24], and orbital energy shift by substituent group [25] have been investigated.

The temperature dependence of the electrical conductance is one of the most basic and important characteristics to understand the charge transport mechanisms.

In the single-molecule junction, tunnel transport is usually dominant. However, thermal hopping charge transport mechanism, i.e., the thermally activated motion of the localized charge injected in a molecule, is also expected to exist. As the thermal hopping transport would open a path to create new device functions such as hysteresis (memory) [26], it is important to clarify the existence of it in the single-molecule junction.

The hopping transport would prevail the tunnel transport at a long distance because the resistance due to the tunnel and hopping transport increases exponentially and linearly, respectively [27]. Temperature dependence of the resistance would give direct evidence for the hopping transport because the tunnel transport is basically a temperature-independent process, although it should be noted that weak temperature dependence can be observed even for the tunnel transport due to thermal excitation of electrons in electrodes [28].

However, it has been difficult to evaluate the temperature dependence because the change of the temperature would cause thermal fluctuations of a molecule and deformations of device structures. The BJ method in which single-molecule junctions are created at each measurement does not suffer from these problems.

The crossover between the tunneling and hopping transport was investigated using oligothiophene molecule (Fig. 2.4a) [29, 30]. The exponential increase of the resistance as a function of the molecular length with $\beta = 1.4\ \mathrm{nm}^{-1}$ is observed between 5 and 14 mer ($m = 1 \sim 4$) which is attributed to the tunnel transport following $R_{tunnel} = R_0 \exp(\beta l)$ where R_0 is constant, β is a tunnel decay constant, and l is molecular length as shown in Fig. 2.4b. The much weaker slope with $\beta = 0.5\ \mathrm{nm}^{-1}$ is observed for longer molecules suggesting the change of the transport mechanism to hopping. In fact, the resistance of the longer molecules shows linear dependence on the molecular length as shown in Fig. 2.4c that is expected for the hopping transport.

To confirm the hopping transport, temperature dependence of the conductance was measured for 5- ($m = 1$), 14- ($m = 4$), 17-mer ($m = 5$) molecules. Figure 2.4d shows the Arrhenius plot of the conductance values measured. The conductance of 5-mer molecule does not show clear temperature dependence, whereas that of 17-mer molecule shows clear temperature dependence with an activation energy of 0.3 eV. The conductance of 14-mer molecule is temperature independent below 300 K and starts to increase as temperature is raised. Above 400 K, the slope in the Arrhenius plot is equivalent to that observed for 17-mer molecule. Their result clearly demonstrated the crossover between tunneling and hopping transport as a function of not only molecular length but also temperature.

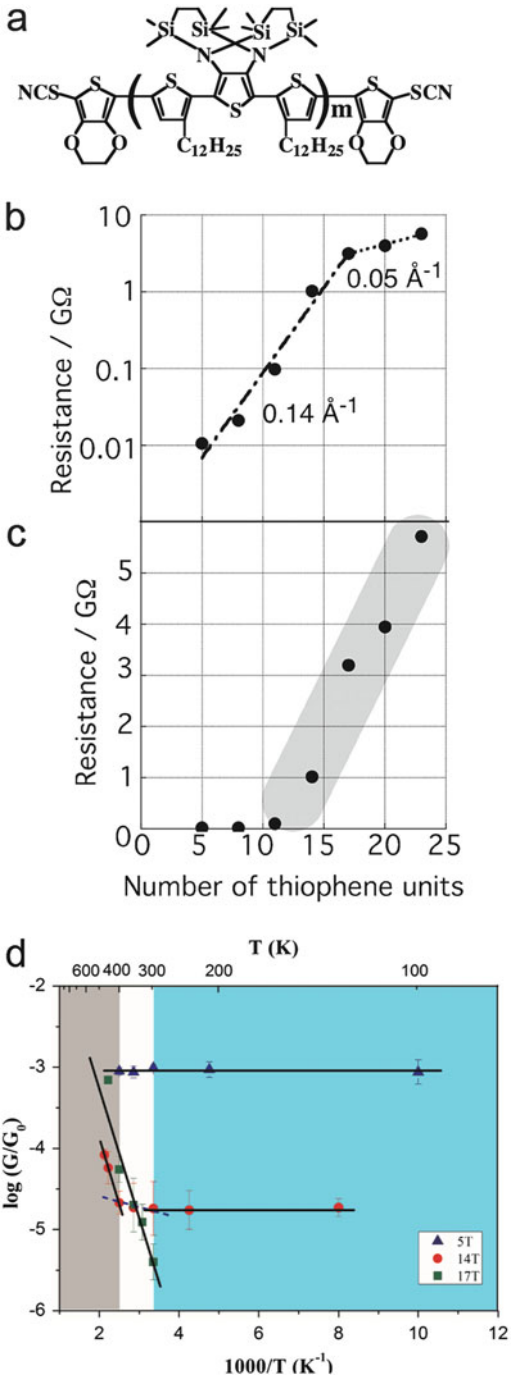

Fig. 2.4 (**a**) The structure of oligothiophene molecule used in the measurement. (**b**), (**c**) show resistance values as a function of molecular length in semilog and linear scale, respectively [29]. (**d**) The Arrhenius plot of the conductance for 5-, 14-, and 17-mer molecules [30]

2.2.1.2 Mechanically Controllable Break Junction

The MCBJ method uses a suspended metal contact fabricated on an elastic substrate as shown in Fig. 2.5a [7–10]. The substrate is placed in the three-point bending machine. The rod (pushing rod) at the center of the substrate is moved vertically by a screw and/or piezo-actuator to bend the substrate. The bending of the substrate elongates and finally breaks the metal contact.

The elastic substrate is usually made of metal sheets such as phosphor bronze and spring stainless steel. The surface of the metal substrate is insulated by polymer, typically polyimide. Then, the metal electrodes are fabricated by either putting metal wires with a notch created by etching or mechanical cutting or micro/nano-lithography process. The latter is more popular because it can achieve higher resolution. In case of using the lithography process to fabricate the electrode, the insulating layer (polyimide) underneath the electrode is etched using the reactive ion etching (RIE) method to make the electrodes suspended (Fig. 2.5b).

The advantage of MCBJ technique is high resolution and stability. The vertical motion of the pushing rod is converted to the lateral motion with an attenuation factor that is determined by the geometry of the chip. With a configuration shown in Fig. 2.5a, the attenuation factor (a) is estimated by $a = \Delta l/\Delta z \sim 6ut/L^2$, where

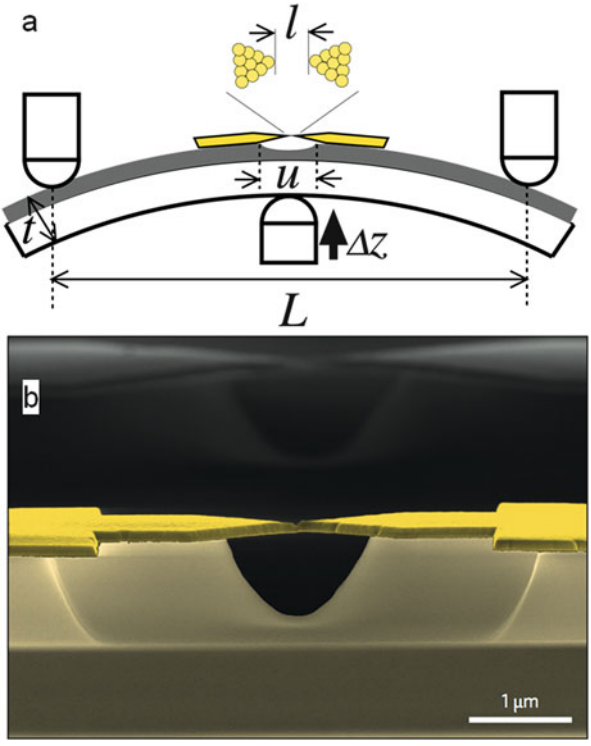

Fig. 2.5 (**a**) A schematic of a MCBJ setup. (**b**) A scanning electron microscopy image of a suspended electrode for MCBJ measurements prepared by lithography and etching technique [58]

Δz is the displacement of the pushing rod, Δl is the change of the gap distance, u is the length of the suspended bridge, t is the thickness of the support materials, and L is the length between two supporting points in the three-point bending configuration [31].

For example, $L = 15$ mm, $u = 4$ μm, and $t = 100$ μm give $a = 10^{-5}$. The pushing rod can be controlled within an accuracy of 1 nm by using piezoelectric actuator, and thus, sub-pm resolution can be achievable theoretically. In addition to the high distance resolution, the MCBJ setup is more robust against external vibrations and thermal fluctuations than STM because mobile parts are assembled in a small space and the bending machine itself can be also designed to be compact which is favorable to make the device mechanically robust and achieve high mechanical resonant frequency.

The resolution of the MCBJ method can be evaluated by measuring the decay of the tunneling current at low bias voltages [32]. The tunneling current (I) at the low bias voltages is described as

$$I \propto \exp\left(-2l\sqrt{2m\phi}/\hbar\right) \sim \exp\left(-10.2l\sqrt{\phi}(eV)^{-0.5}\ \mathrm{nm}^{-1}\right),$$

where l is the gap distance, m is the electron effective mass, and ϕ is the tunneling barrier height. The decay of the tunneling current from I_1 to I_2 according to the change of the gap distance from l_1 to l_2 is expressed as

$$I_1/I_2 \propto \exp\left\{-10.2\ (l_1 - l_2)\sqrt{\varphi}\ (eV)^{-0.5}\ \mathrm{nm}^{-1}\right\}$$

By fitting the observed current decay as a function of the motion of the pushing rod with assuming barrier height to be a few eV, the actual attenuation factor can be obtained. Typically, actual distance resolution of MCBJ method is in the order of tens of pm.

Due to the high distance resolution and stability, MCBJ is frequently used to measure current-voltage characteristics of the single-molecule junctions. Figure 2.6 shows results on current-voltage (IV) measurements of 9,10-dihydroanthracene bridged between gold electrodes carried out under the elongation of the gap distance at 6 K [33]. The IV characteristics show negative differential resistance (NDR) which is caused by breaking of the resonance tunneling between two π-conjugating units under the bias voltage as shown in Fig. 2.6a. As the gap distance increases, the NDR is weakened and disappeared. The stable IV measurements under precise control of the gap distance allows us to create the conductance transient by plotting the conductance determined from the IV characteristics at low bias regions as shown in Fig. 2.6b and to find the relation between NDR behaviors and structure of the conductance plateaus which will be helpful to understand the structure of the junction. Also, detailed IV characteristics and other interesting transport properties such as inelastic tunneling spectroscopy and noise spectroscopy are measured, which is discussed in Chap. 3.

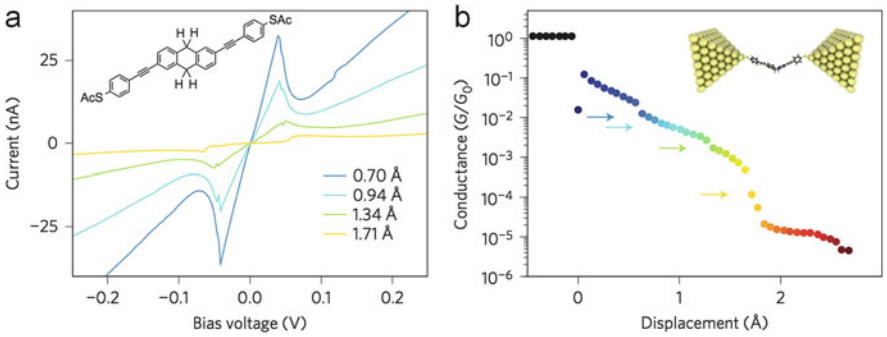

Fig. 2.6 (**a**) Current-voltage characteristics of the single-molecule junction of 9,10-dihydroanthracene using gold electrodes as a function of different gap separations at 6 K. Inset shows the structure of the molecule. (**b**) A conductance transient curve created from the IV characteristics at different gap distances. *Colored arrows* show positions where the current-voltage curves with the same color in (*a*) are taken [33]

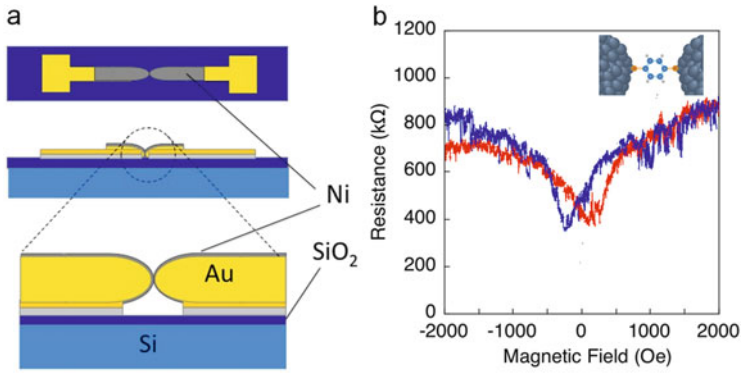

Fig. 2.7 (**a**) A schematic of a structure of the electrode used to measure MR effect in the MCBJ setup. (**b**) Resistance as a function of external magnetic fields (MR loop) observed for a benzenedithiol single-molecule junction using Ni electrodes

MCBJ is also useful to measure effects of external fields on the charge transport characteristics such as magnetic and electrostatic fields. However, the mechanical deformations of the electrodes caused by the external fields should be avoided. For example, to measure the magnetic field effects on single-molecule junctions using ferromagnetic electrodes (magnetoresistance (MR)), mechanical deformations of the electrode due to magnetic force and magnetostriction should be avoided [34, 35].

Figure 2.7a shows the structure of the electrode used to measure the MR effect of single-molecule junctions using Ni electrodes [36]. Initially gold electrodes with a gap separation of 4 μm were prepared by conventional photolithography. Then, the gap separation was reduced to ∼0.5 μm by electrodeposition of gold onto the electrode pattern. Then, a ferromagnetic layer (Ni) was electrochemically deposited

to form a nano-contact of Ni. In this electrode structure, the supporting gold electrodes are robust enough to avoid the deformation due to the magnetic fields, and the Ni layer is thin enough to remove the effect due to magnetostriction. By using this device structure, MR loop is successfully measured as shown in Fig. 2.7b. Device structures for electrostatic field will be explained in Sect. 2.3.3.

2.2.2 Statistical Data Analysis

Since the current transient measured during the break junction process can be originated from various junction structures formed during the breaking process, a statistical analysis is usually used to determine the conductance of a single-molecule junction. The statistical analysis also reveals useful information such as sequences of the structures appearing during the breaking process. In this section, typical analysis methods in addition to the conductance histogram are explained.

2.2.2.1 Distance and Conductance: Two-Dimensional Histogram

The conductance transient curves contain information not only on conductance but also on distance. Since changes of the gap distance can alter structures of a single-molecule junction, dependence of conductance values on the gap distance would give fruitful information on the structure of the single-molecule junction. Two-dimensional (2D) histograms are useful to analyze distribution of the conductance as a function of gap distance (or stretching length) [37].

Figure 2.8a shows conductance histogram obtained for 4,4′-bipyridine using gold electrodes [38], showing two peaks as indicated as low and high. The conductance transients (Fig. 2.8b) show a trend that the low conductance plateaus appear after the high conductance plateaus.

The distance distribution of the high and low conductance states is evident in the conductance 2D histogram shown in Fig. 2.8c. In the 2D histogram, the number of data points at a certain conductance and distance is counted and shown as a color map. A huge peak is observed around the position where the displacement is 0.2 nm and the conductance is 10^{-3} G_0 which corresponds to the high conductance state observed in the conductance histogram shown in Fig. 2.8a. The small peak which corresponds to the low conductance state is observed just below the huge peak. From this 2D histogram, it is found that the high conductance state appears just after the breaking of the junction, whereas the low conductance state appears after the gap distance is separated more than 0.2 nm. In fact, these two conductance states can be reversibly switched by controlling the gap distance as shown in Fig. 2.8d. With the help of theoretical calculation, the transition between the high and low conductance states is attributed to the sliding of the bonding site of nitrogen on the gold tip (Fig. 2.8e).

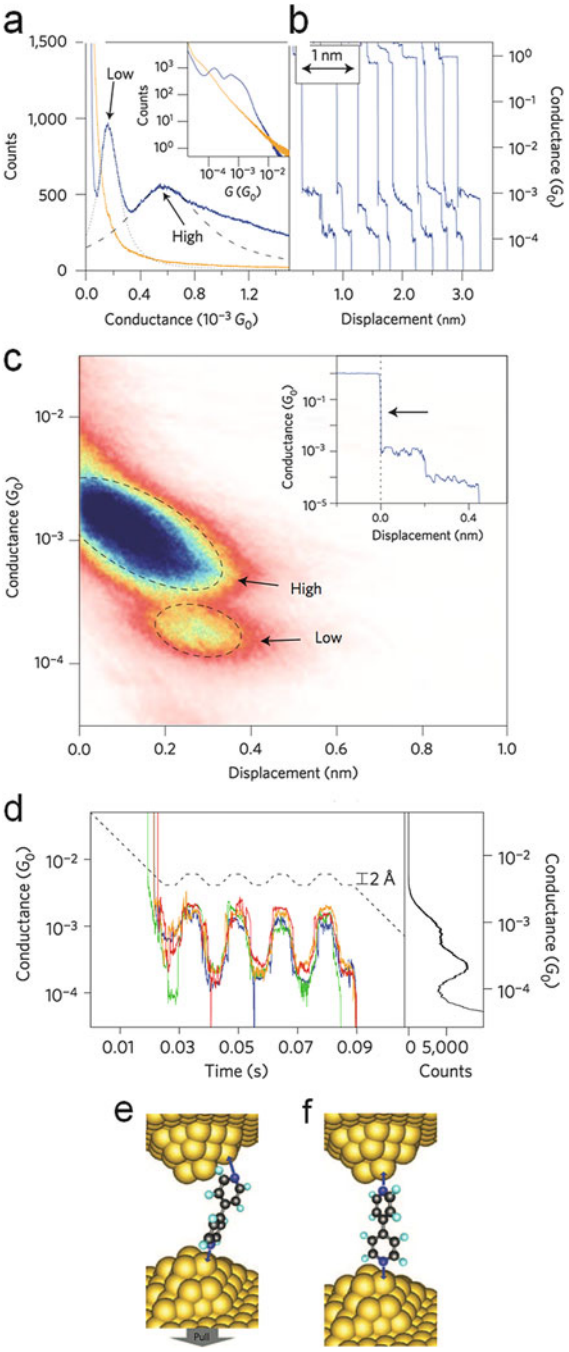

Fig. 2.8 Conductance histogram (**a**) and transient curves (**b**) observed for 4,4′-bipyridine using gold electrodes. (**c**) 2D histogram of the conductance transient curves observed. The displacement is measured with respect to the position where the conductance drops from 1 G_0. (**d**) Conductance measured with a distance modulation showing reversible conductance switching between high and low conductance states. *Dashed curve* represents motion of the STM tip. The colored curves show the conductance measured in different experiments. (**e**) Schematic models of the junction for high and low conductance states [38]

2.2.2.2 Cross Correlation and Conditional Histogram Analysis

The conductance transient curves contain information on dynamics of the junction formation. For example, in the molecular mechanical switch shown in Fig. 2.8, the low conductance plateau appears following to the high conductance plateau. This kind of correlation between different conductance values is useful to understand the formation dynamics of the junction and is evaluated by cross correlation analysis in which correlation between each bin of the conductance histogram for all conductance transient curves is evaluated. In this section, the interpretation of the cross correlation analysis is briefly explained by some examples because methods to create cross correlation histogram are too technical to be explained here. For more details, readers may refer other articles [39–41].

Figure 2.9a, b shows the conductance transient and histogram observed between Co tip and Ge substrate, respectively [39]. The conductance histogram reveals several sharp peaks indicated by *a*-*g*. The conductance transient curves tend to have certain sets of sequence of the plateaus, such as *f*-*c*-*a* and *f*-*d*-*a*.

This trend is clearly resolved in cross correlation histogram shown in Fig. 2.9c. In this histogram, the co-relation between two conductance values indicated in horizontal and vertical axes is shown. White color (or bright area) corresponds to positive values. The peaks at diagonal correspond to the peaks in the conductance histogram shown in Fig. 2.9b. For example, when one looks at the horizontal position at the conductance peak *a*, a strong peak is found at the location of the peak c. On the other hand, there are no peaks observed at location of the peak b. This result indicates that the peak c appears in accordance with the peak a but not b.

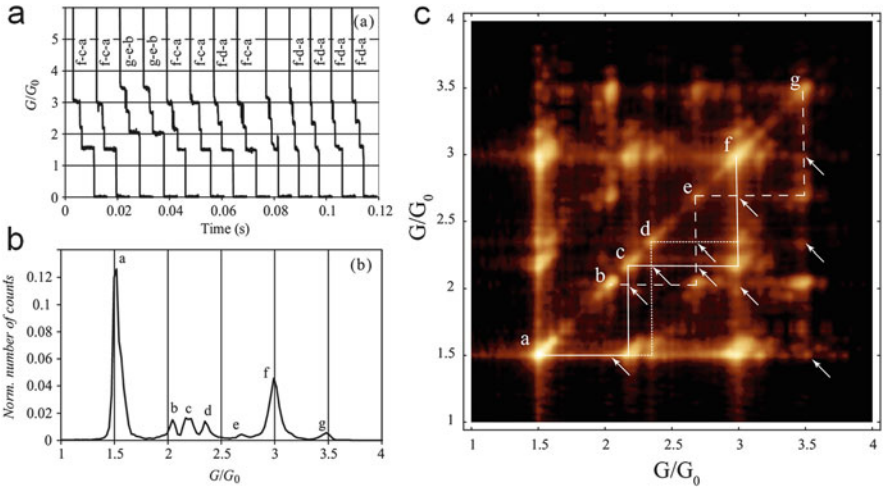

Fig. 2.9 Conductance transient curves (**a**) and histogram (**b**) obtained for Co-Ge junction. (**c**) Conductance co-relation histogram. Typical scenarios of breaking sequence are indicated by *solid*, *dotted*, and *dashed lines* [39]

We can also find a peak between the peak c and the peak f. Therefore, a sequence f-c-a is expected during the break junction process. Similarly, sequences g-e-b and f-d-a are identified. This analysis gives information on the formation dynamic of the junction.

The detailed analysis of the cross correlation on the break junction data revealed that the cross correlation histogram shows not only the correlation in the occurrence of the plateau but also that of the plateau lengths. Although two conductance values are correlated in occurrence, the cross correlation value can be negative due to negative correlation in plateau length, e.g., long plateau followed by short plateau. The correlation in the occurrence can be evaluated by creating conditional histograms that are made from data sets contributing to certain histogram peaks of interest [40]. If two histogram peaks, A, B, posses anticorrelation (correlation) in occurrence, the histogram created from the data contributing to peak A does not (does) show peak B. The histogram created in this manner is called conditional histogram.

Figure 2.10 show an example of correlation analysis on 4,4′-bipyridine molecule junction shown in Fig. 2.8 [40]. The conductance histogram (Fig. 2.10a, black shadowed) shows two distinct peaks. The cross correlation histogram (Fig. 2.10c) shows negative value for these two peaks, which indicates anticorrelation of

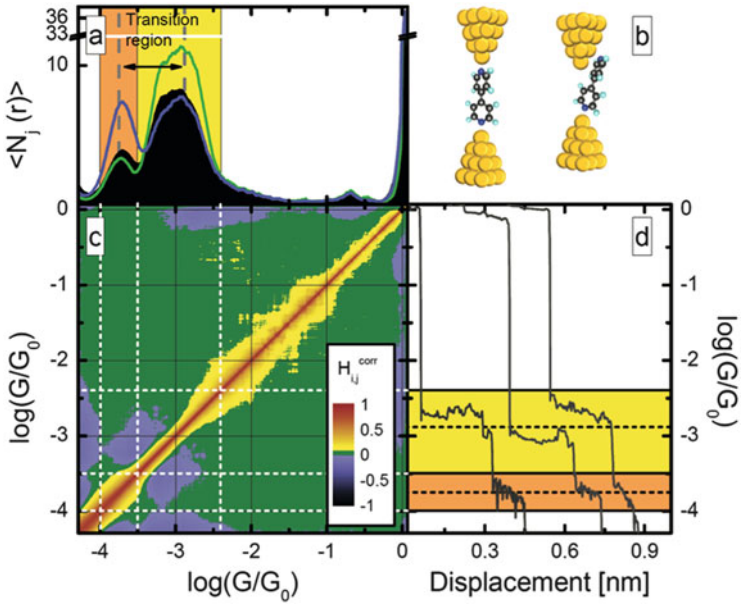

Fig. 2.10 Correlation analysis of the conductance of 4,4′-bipyridine molecule junction using gold electrodes. (**a**) Whole conductance histogram (*black shaded*) and conditional histogram for low conductance (*green line*) and high conductance (*blue line*). (**b**) Proposed model for high and low conductance states. (**c**) Two-dimensional correlation histogram. (**d**) Typical conductance transient curves [40]

occurrence or plateau length. As the conditional histogram for the small conductance peak (Fig. 2.10a, blue curve) shows high conductance peak and vice versa, the negative correlation is attributed to the anticorrelation of plateau length. Therefore, the correlation in occurrence exists between the high and low conductance states which support the proposed mechanism of the conductance switching.

2.2.3 Related Techniques

2.2.3.1 Distance Modulations

In the break junction measurement, formations of single-molecule junctions are detected by the conductance plateaus that can be basically evident only after the breaking of the junctions. A distance modulation technique [42] provides useful information on the formation of the single-molecule junctions and convenient especially when one would like to conduct static measurements such as current-voltage measurements on a single-molecule junction.

In this technique, the distance between two electrodes is modulated at a certain frequency and the AC component of the current synchronizing to the gap distance modulation is measured. In brief, when a current (I) is measured at a gap distance ($D = d_0$), the amplitude of the AC current corresponds to $\mathrm{d}I/\mathrm{d}D$ at d_0 that should be close to 0 where the conductance plateau is formed.

The total current I is described as

$$I = I_{\mathrm{DC}} + \mathrm{d}I/\mathrm{d}D \ \ \mathrm{A}_0 \cos \ \ \omega t,$$

where I_{DC}, A_0, and ω are the measured DC current, amplitude of the distance modulation, and angular frequency, respectively.

First of all, the expression for $\mathrm{d}I/\mathrm{d}D$ in case of the vacuum tunneling is discussed. In this case, this technique is equal to the barrier height measurement used in the conventional STM measurement [43]:

$$I_{\mathrm{DC}} \sim I_0 \exp\left(-\beta D\right),$$

where β is the tunneling decay constant and I_0 is a constant.

$$\mathrm{d}I_{\mathrm{DC}}/\mathrm{d}D = -I_0 \ \beta \ \ \exp\left(-\beta D\right) = -\beta I_{\mathrm{DC}}$$

Therefore,

$$\beta = -\mathrm{d}I/\mathrm{d}D/I_{\mathrm{DC}}$$

In the single-molecule junction, the current response with respect to distance is not expressed by a simple equation because it can contain various effects such as

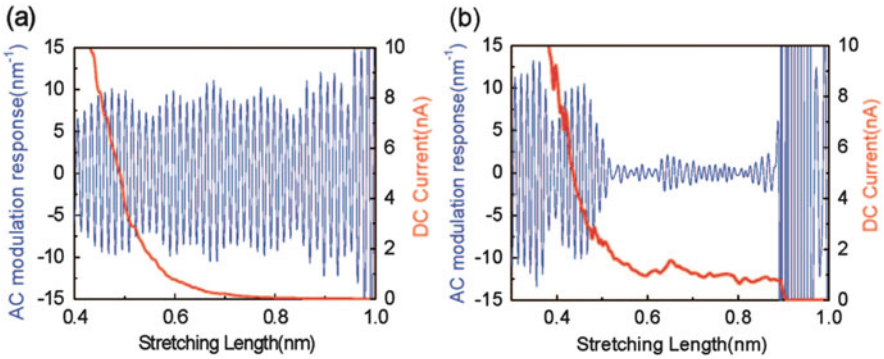

Fig. 2.11 I_{DC} (*red*) and I_{AC}/I_{DC} (*blue*) measured in the break junction measurement without (**a**) and with (**b**) the presence of 1,8′-octanedithiol. The amplitude or peak value of I_{AC}/I_{DC} gives α [42]

mechanical elongation of the junctions and piezoelectric response of molecules [44]. However, dI/dD/I_{DC} is still a convenient parameter to describe mechanical response of the single-molecule junction since dI/dD should be normalized and referred as α.

Figure 2.11 shows I_{DC} and I_{AC}/I_{DC} whose amplitude represents α observed in the experiment using 1,8′-octanedithol [42]. When no molecules are contained in the measurement system (Fig. 2.11a), only exponential decay of I_{DC} and almost constant α are observed. In the presence of 1,8′-octadecanedithiol (Fig. 2.11b), I_{DC} shows stepwise changes (plateaus) and α becomes small at the plateau region. After the break down of the plateau, α suddenly increased. These results demonstrate α is a good indicator to monitor the formation of the single-molecule junctions.

The ability of the distance modulation technique was demonstrated in the measurements of a molecular diode [45]. It is necessary to know the orientation of the molecular diode with respect to the bias voltage to understand the rectification behavior. However, it is not possible to maintain or identify the orientation of the molecule in the break junction measurement. Therefore, the measurement was conducted by gently contacting the STM tip to the surface of the self-assembled monolayer of the diode molecule whose orientation is controlled by a sequential two-step chemical deprotection method as shown in Fig. 2.12a. When the position of the STM tip is held at the conductance of the single diode molecule determined by the conventional break junction method, the alpha and I_{DC} stochastically change (Fig. 2.12b). The jump of Idc to higher value is accompanied by the jump of alpha to smaller value, which indicates the formation of the molecule junction, allowing the detection of the formation of the molecule junctions. The current-voltage characteristic is measured when the junction is formed (Fig. 2.12b). The modulation in parallel to the substrate in the STM setup is used to evaluate the lateral coupling between molecules and substrate [46].

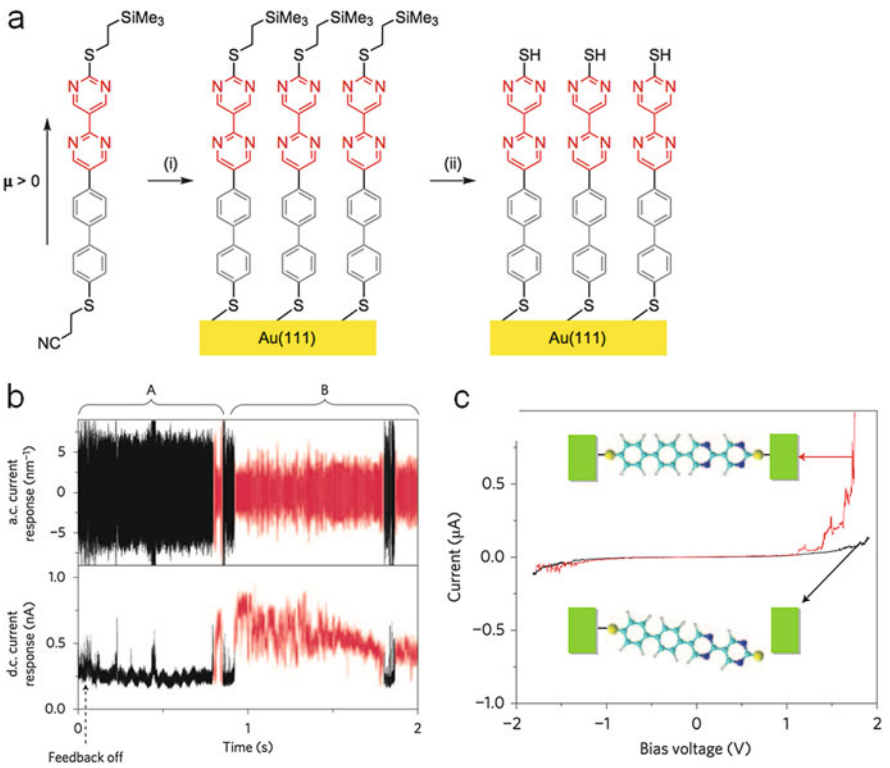

Fig. 2.12 (**a**) A method to prepare a monolayer of diode molecule (dipyrimidinyl-diphenyl molecule). A thiol group at the top of the molecule in the figure is deactivated by a protecting group so that the molecules adsorbed only through sulfur atoms at the bottom end of the molecule (step I). After the formation of the monolayer, the protecting group is chemically detached and SH groups which can bind to metal electrodes is generated on *top* of the molecule. (**b**) I_{AC}/I_{DC} and I_{DC} measured. The gap distance was held during the measurement. (**c**) Current-voltage characteristics measured at the region A (*black*) and B (*red*) in (*b*), which corresponds to the junction with a tunnel gap and the single-molecule junction, respectively [45]

2.2.3.2 Electromechanical Responses

The breaking process of the junction is studied in more detail by using an atomic force microscope (AFM) [47–51]. The force observed during the breaking process combined with the electrical conductance gives information on the bonding structure between molecules and electrodes. This measurement is also interesting to understand changes of electrical characteristics caused by mechanical perturbations, i.e., electromechanical responses, of the single-molecule junction that can be used to design single-molecule electronic devices. In this section, the procedure and an example of the measurement are briefly introduced. More detailed discussion is given in Chap. 3.

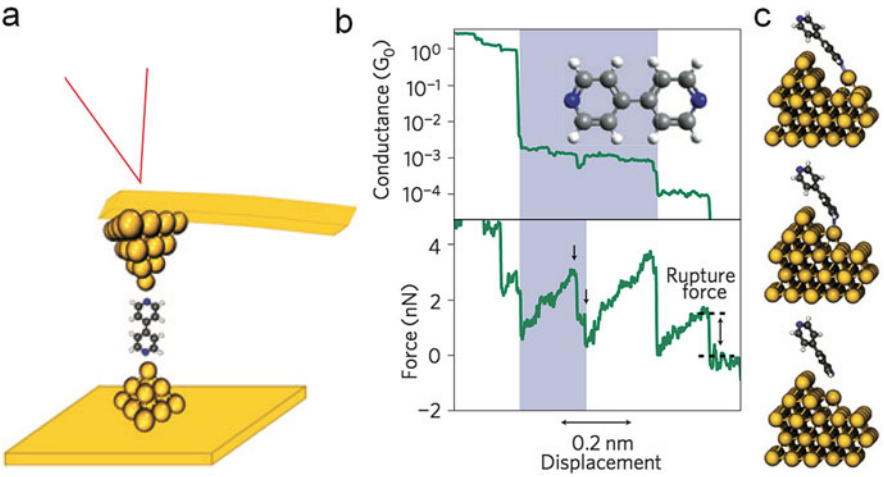

Fig. 2.13 (**a**) A schematic of the AFM-BJ method. The deflection of the cantilever is monitored by the position of a laser reflected from the backside of the cantilever. The bias voltage is applied between the tip and the substrate. (**b**) A conductance transient curve obtained for 4,4′-bypyridine junction using Au electrodes and force measured simultaneously. (**c**) Model structures representing the force rupture event observed in the middle of the conductance plateau indicated by *arrows* [50]

Figure 2.13a shows a scheme of the measurement system. The BJ measurement is carried out with a metal-coated AFM tip. The force acting on the tip is measured from the deflection of a cantilever by a conventional AFM setup. A bias voltage is applied between the AFM tip and the substrate and electrical current is measured simultaneously with the force.

Figure 2.13b shows the conductance and force transient obtained for 4,4′-bypyridine junction using Au electrode [50]. The conductance transient shows clear two-step plateaus and sharp decrease of force is observed at the conductance steps where the bonding between molecules and electrodes is broken. In addition, another sharp drop in the force transient is observed in the middle of the first long conductance plateau at 10^{-3} G_0 where a small dip of the conductance is observed. This result indicates that structural changes of the molecule junction without causing significant changes in the conductance can be detected by the force measurement. A proposed model for this structural change is shown in Fig. 2.13c. After the breaking of the gold atomic contact, the molecule can bind to rough gold surface through both specific bonding through N atom and van der Waals interaction through carbon ring. Upon elongation of the gap distance, the van der Waals bonding raptures and causes a drop of force, whereas the conductance does not change a lot. More detailed and quantitative analysis of the rupture force can be used to deduce the strength of the bonding between electrode and molecule as discussed in Chap. 3.

2.2.3.3 Electrical and Electrolyte Gating

An application of an electrostatic gate field shifts the energy of the system and hence the transport characteristics. When the junction is positively (negatively) charged, the energy levels would be shifted to higher (lower) levels (Fig. 2.14a, b). The gate effect is not only useful to investigate transport mechanism but also an important step to realize active devices [52]. Fabrication of a solid-state gate electrode to nm-scale junctions such as shown in Fig. 2.14c is still challenging [53]. To prepare single-molecule junctions on solid-state gate electrodes, electromigration which is explained in Sect. 3.1 and shadow mask techniques [54] have been used. However, application of gate electric fields in the MCBJ setup has been desired.

When electric field is applied to source and drain electrodes from a gate electrode placed underneath them in the MCBJ setup (Fig. 2.15a), electrostatic force causes deformations of the cantilever-shape source and drain electrodes, and the atomic contact can be reversibly opened and closed by the application of gate field as shown in Fig. 2.15b [55]. A side gate structure was developed by electron-beam lithography as shown in Fig. 2.15c [56]. However, the distance, typically in the order of tens of nm, between the gate electrode and the molecule junction is too large

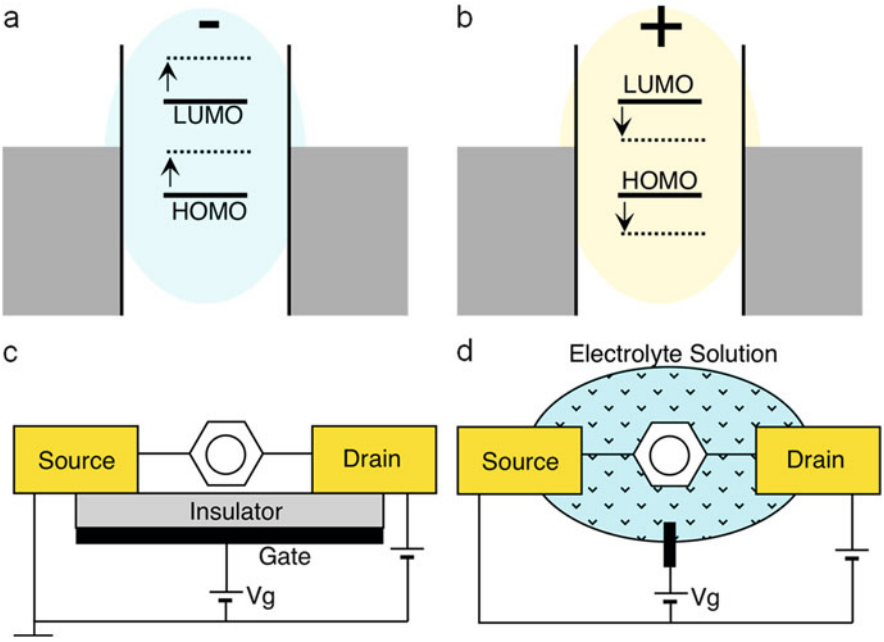

Fig. 2.14 Energy shifts of a molecule junction when negatively gated (**a**) and positively gated (**b**). Schemes for solid-state gate (**c**) and electrolyte gate (**d**). HOMO and LUMO represent highest occupied and lowest unoccupied molecular orbitals, respectively

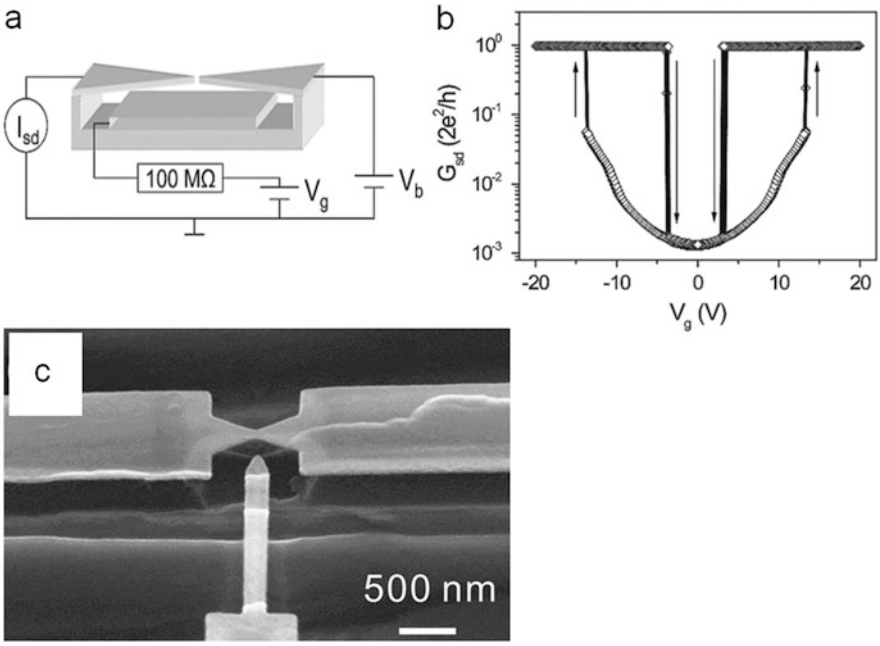

Fig. 2.15 (**a**) Schematic of the device structure and measurement circuit. (**b**) Switching characteristics of the device under the application of the gate voltage. (**c**) A scanning electron microscopy image of a MCBJ device with a side gate. (**a**), (**b**) [55,56]

to generate electric fields effective to tune the electronic structure of the molecule junctions.

To realize the effective electrostatic gate effect without deformation of the source and drain electrodes, the sandwich-type electrode structure was developed [57, 58]. In this structure, the source and drain electrodes are fabricated on the gate electrode covered with aluminum oxide layer and whole electrode is suspended (Fig. 2.16a). Under the bending of the supporting substrate, only the source and drain electrode can be broken allowing the BJ measurement.

Performance of the MCBJ with the stacked gate electrode is demonstrated by using the thiol-terminated zinc-porphyrin molecule [Zn(5,15-di(p-thiolphenyl)-10,20-di(p-tolyl)porphyrin)] (ZnTPPdT) (Fig. 2.16b) [58]. The current-voltage characteristics of the single-molecule junction of ZnTPPdT shows Coulomb blockade as shown in (Fig. 2.16c). Figure 2.16d and e shows color maps of the differential conductance under the application of the source and drain voltages and gate voltages. Note that peaks appearing in the differential conductance correspond to the voltages where the current start to increase in the current-voltage characteristics shown in Fig. 2.16c and, thus, energy levels of transport channels. Figure 2.16d shows peak shifts to higher energy under the application of positive gate voltages, whereas peak shifts toward lower energy is observed in Fig. 2.16e. The observed

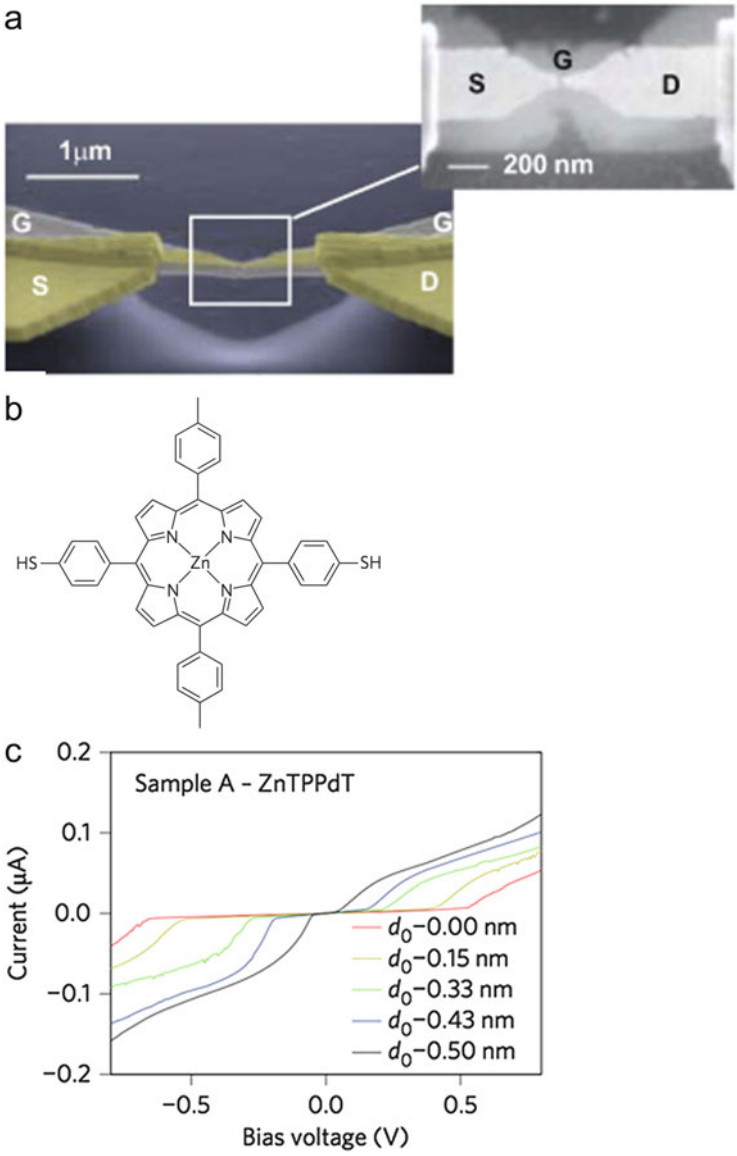

Fig. 2.16 (**a**) Scanning electron microscopy images of a MCBJ electrode. A gate electrode is attached underneath suspended source (*S*) and drain (*D*) electrodes through an oxide layer [57]. (**b**) Structure of ZnTPPdT. (**c**) Typical current-voltage characteristics of the single-molecule junction of zinc porphyrin measured at various gap separations showing Coulomb blockade. (**d**), (**e**) dI/dV color maps under the application of gate voltages (horizontal axis) and source-drain voltage (vertical axis). (**f**) An energy diagram showing the effect of a gate voltage, Vg. The *b* in the figure represents the effective gate coupling strength which is used to estimate the effective electrostatic field from the applied gate voltage [58]

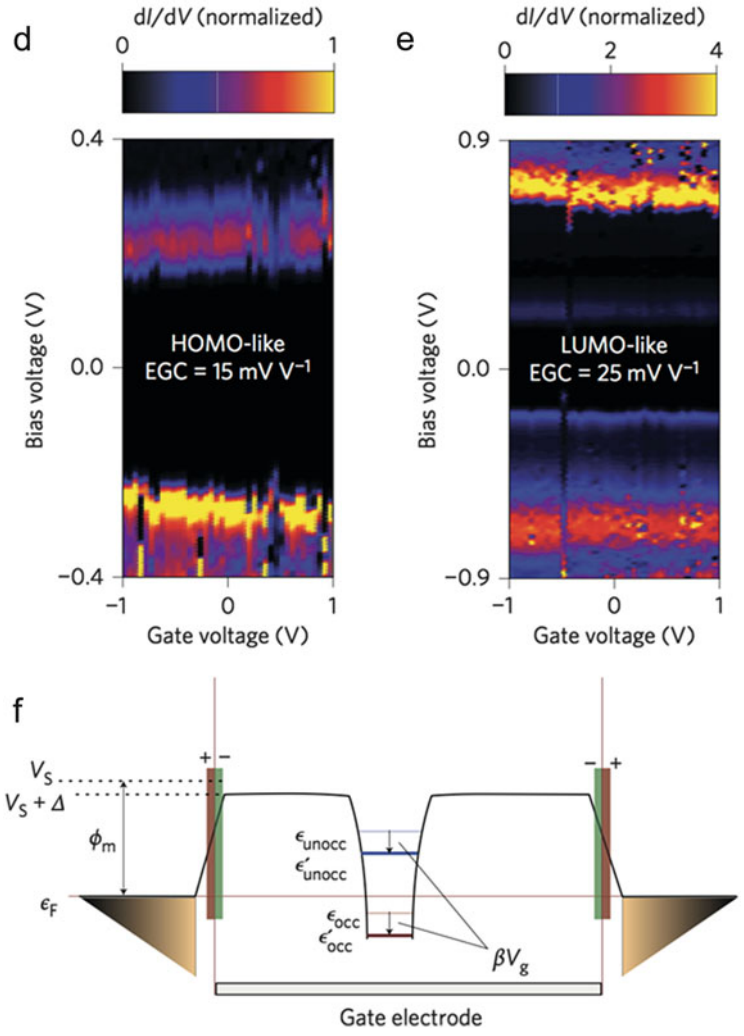

Fig. 2.16 (continued)

behavior is explained using energy diagram shown in Fig. 2.16f. When positive gate voltage is applied, energy levels in the molecule are shifted to lower energy. The downward shift opens the gap between Fermi level and highest occupied molecular orbital (HOMO)-like transport channel, resulting in the shift of the peak in differential conductance toward higher energy, which is observed in Fig. 2.16d. On the contrary, the gap between Fermi level and lowest unoccupied molecular orbital (LUMO)-like transport channel would become small under the application of positive gate voltage, which is observed in Fig. 2.16e. Note that HOMO-like and LUMO-like indicate the energy levels of the molecule in the junction used for the

charge transport that does not always correspond to the HOMO and LUMO of the molecule in gas phase.

The electric field effect can be also studied by using electrochemical environment, i.e., in electrolyte solutions, as shown in Fig. 2.14d [59]. In this method, the gate electric field (electrochemical potential) is applied through the electric double layer formed by ions in the solution. In terms of electrochemistry, electrochemical potentials of source and drain electrodes are controlled with respect to the reference electrode put in the solution. There are two possible gating mechanisms in electrochemical environment. One of the mechanisms uses the electric field applied through electric double layers formed by ions whose thickness can be reduced in the order of 0.1 nm, allowing the generation of strong electric field for the gating. In the electrochemistry term, this process corresponds to the potential scan in the so-called double-layer region where no electrochemical reactions (or Faradic current) take place. In another mechanism, the electrochemical reaction of the molecule takes place, i.e., the electronic state of the junction is tuned by the charge injection into the molecule. The former and the latter are sometimes referred as electrolyte and electrochemical gating, respectively.

The electrolyte gating is convenient because it can be applicable for both STM-BJ and MCBJ. However, one should pay attention that the charge transport mechanism can be affected by polar solvents. For example, single-molecule junctions of perylene tetracarboxylic diimide (PTCDI) derivatives show temperature-independent tunneling transport and temperature-dependent hopping transport in nonpolar and polar solvent, respectively [60].

2.3 Other Experimental Methods to Prepare Single-Molecule Junctions

2.3.1 Electromigration Technique

When sufficient electrical current is applied in a narrow metal wire and a critical temperature is reached by Joule heating, metal atoms in the metal wire become mobile and start to drift due to the transfer of momentum of electron [53, 61]. The drift of the metal atoms results in the gradual reduction of the size of the wire and eventually formation of atomic contact and a gap. This process is called electromigration.

To fabricate a gapped electrode by this technique, a necked wire pattern is prepared where the gap should be created (Fig. 2.17a). When a voltage applied to the wire is increased, the electrical current starts to collapse at a certain voltage (Fig. 2.17b, denoted 1) where the electromigration process begins. The voltage should be quickly decreased to avoid the catastrophic breaking of the wire (Fig. 2.17b, denoted 2–3) and then increased again to cause the next electromigration process (Fig. 2.17b, denoted 4). By repeating this cycle, the wire is narrowed to reach atomic size and finally a gap is formed. This process can be monitored

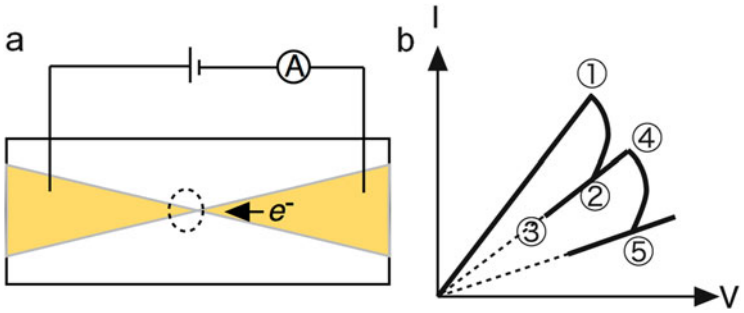

Fig. 2.17 (**a**) Scheme of an electrode subjected to the electromigration. Atoms at the necked region will be stacked around the area indicated by a *dotted circle*. (**b**) A scheme of electrical current observed under the successive electromigration process

from the stepwise decrease of the conductance by a quantum conductance after the electromigration process. A fast feedback control of the electrical power during the electromigration process followed by spontaneous self-breaking of atomic contacts enables researchers to prepare an atomic contact and an electrode gap with a separation of a few or less than nm [62–64]. When molecules are adsorbed on metal electrodes before breaking, molecule junctions can be formed after the breaking of the wire.

The advantage of this technique is that one can prepare single-molecule junctions on a gate insulator as explained in detail below. The disadvantages are as follows: fake signals are sometimes obtained by metal particles and grains generated in electromigration process [65]; yield of molecule junction is low, typically a few %; and the conductance of a single-molecule junction should be determined by different techniques such as the BJ techniques.

Using electromigration techniques, a single-molecule junction can be prepared on a gate insulator as schematically shown in Fig. 2.18 inset [66]. In this structure, an electrode pattern subjected to the electromigration process is fabricated on an Al_2O_3 layer formed on an Al electrode which is used as a gate electrode. The electromigration was performed to prepare molecule junctions of 1,4-benzenedithiol (BDT). The formation of the molecule junction is confirmed by inelastic tunneling spectroscopy (IETS) that is explained in Chap. 3. The gate-modulated current-voltage characteristics were successfully observed as shown in Fig. 2.18.

The electromigration technique may have a potential for a mass production of gap arrays with a separation less than 1 nm which is difficult to be fabricated by

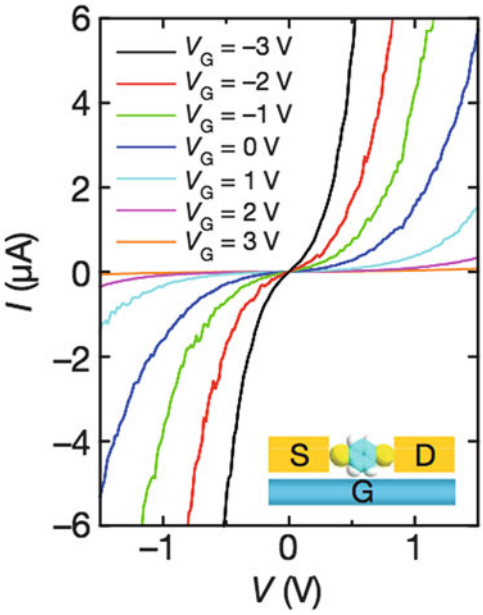

Fig. 2.18 Schematic of device (inset) and current-voltage characteristics of a BDT molecule junction at various gate voltages. *S* and *D* represents source and drain electrodes created by the electromigration of the gold electrode. *G* represents Al gate electrode. An Al_2O_3 layer is formed on the Al electrode by oxidation [66]

lithographic technique since sophisticated methods avoiding generation of metal nanoparticles are developed [63, 64]. The technique to control crystallinity of the electrode edge is under progress [67]. Moreover, this technique is utilized to create a novel lateral in-plane nano-hole that allows single molecules to flow in it [68]. Figure 2.19 shows the device structure. The electrode for the electromigration is sandwiched between oxide insulating layers. When the electrical current is applied, the electrode is narrowed by electromigration process. The gold atoms drift in the space confined by two insulating layers and spill over at the side of the electrode pattern (Fig. 2.19c). After the resistance of the metal electrode becomes higher than 1 kΩ, the bias voltage is held at 0.1 V to cause spontaneous breaking of the electrode which results in the formation of regulated gap fitting to a size of single molecules [64]. By combining a fluidic channel fitting to this structure, single molecules passing through the gap in solutions are detected by measuring the electrical current between the gap. Identification of molecules is possible by analyzing the current. This technique opens a new application field for single-molecule electrical measurement techniques as an analytical tool for single molecules as explained in Chap. 9.

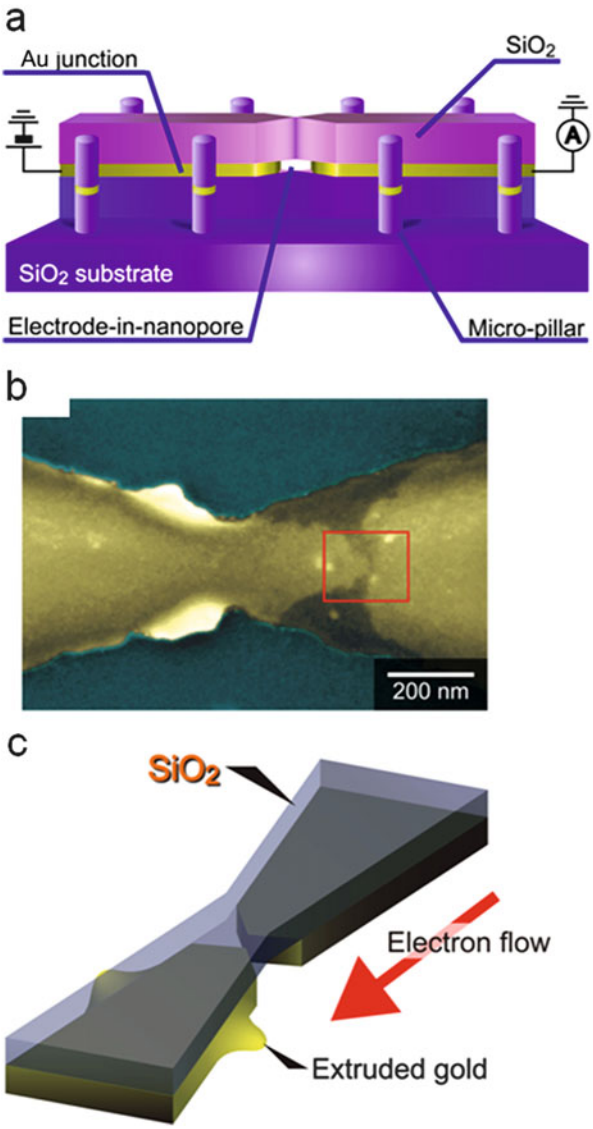

Fig. 2.19 (**a**) Scheme of the device to create an in-plane nano-hole. Thickness of a gold layer is 15 nm. (**b**) A scanning electron microscopy image of the junction subjected to the electromigration process followed by spontaneous breaking. (**c**) Scheme of the junction imaged in (*b*) [68]

2.3.2 *Ultrahigh-Vacuum and Low-Temperature Scanning Tunneling Microscope*

A scanning tunneling microscope (STM) is a powerful technique to observe surfaces with atomic resolution in real space. It is, therefore, natural to use STM to measure electrical properties of single-molecule junctions. Although the stability of the instruments has been an issue, recently, commercial ultrahigh-vacuum low-

temperature (UHV-LT) STM possesses sufficient stability to create, maintain, and measure single-molecule junctions. The advantages of UHV-LT-STM are as follows: one of the electrodes can be a single-crystal surface, i.e., a well-defined structure; the existence of a molecule is confirmed directly by imaging; the location of the electrical contact in the molecule is controlled with intramolecular resolution; and the position of molecules can be manipulated on a surface. The possible drawbacks of UHV-LT-STM are as follows: it requires ultraclean environments and low temperature that requires very specialized and sophisticated knowledge and techniques; it is very time consuming, e.g., a surface should be imaged to find molecules which takes hours; and good probe tip conditions are needed for reliable measurements, which is always the case for UHV-LT-STM measurements.

In this section, some remarkable examples showing the benefit of UHV-LT-STM are briefly explained. For basic principles and mechanism of STM, readers might refer other books [69].

Manipulation of atoms and molecules is one of the fascinating and unique capabilities of UHV-LT-STM that enables researchers to investigate effects of surrounding molecules on the conductance of a single-molecule junction. Figure 2.20a shows STM images of three phenol molecules adsorbed on Cu(110) surface taken at 4.5 K [70]. The three bright spots represent each phenol molecule. The dark area observed at the right of the bright spots in Fig. 2.20a corresponds to the oxygen of phenol from which orientation of molecules can be identified. The lattice lines indicate the position of Cu atoms. Two molecules sit next to each other and one molecule is isolated. When the STM tip is approached to the molecule indicated by 1 in Fig. 2.20a, the tunneling current suddenly jumps up to around 35 nA as shown in the curve 1 in Fig. 2.20c. At this point, the molecule 1 adsorbed on the STM tip by π-bonding of benzene ring and STM tip. When the same measurement was carried out on the molecule 3, i.e., the isolated molecule, the current reaches around 40 nA. This result indicates the neighboring molecule reduced the conductance of the molecule. To make sure the molecule 1 is identical to the molecule 3, the neighboring molecule was flipped to be separated from the molecule 1. The flip of the molecule can be done by lifting the molecule by approaching the tip and then moving laterally. Now, the molecule 1 is isolated as shown in Fig. 2.20b and indicated as 2. When the molecule junction is formed using the molecule 2, the measured current is the same with that observed for the molecule 3. This result clearly demonstrates the effect of neighboring molecules on the conductance of the single-molecule junction. The energy level shift caused by the electrostatic potential of neighboring molecules including dipole moment is attributed to the reduction of the conductance.

A difficult issue in handing single molecules with UHV-LT-STM is sample preparation. Most of the measurements are limited to molecules that can be sublimated in vacuum conditions. Although techniques to introduce large molecules into vacuum, such as pulse valve [71] and electrospray [72, 73], were developed, it is difficult to find right conditions to put molecules on the substrate without damages and contaminations.

For studies of large molecules by STM, on-surface polymerization is useful [74–76]. In this technique, firstly, unit molecular structures that can be sublimated are

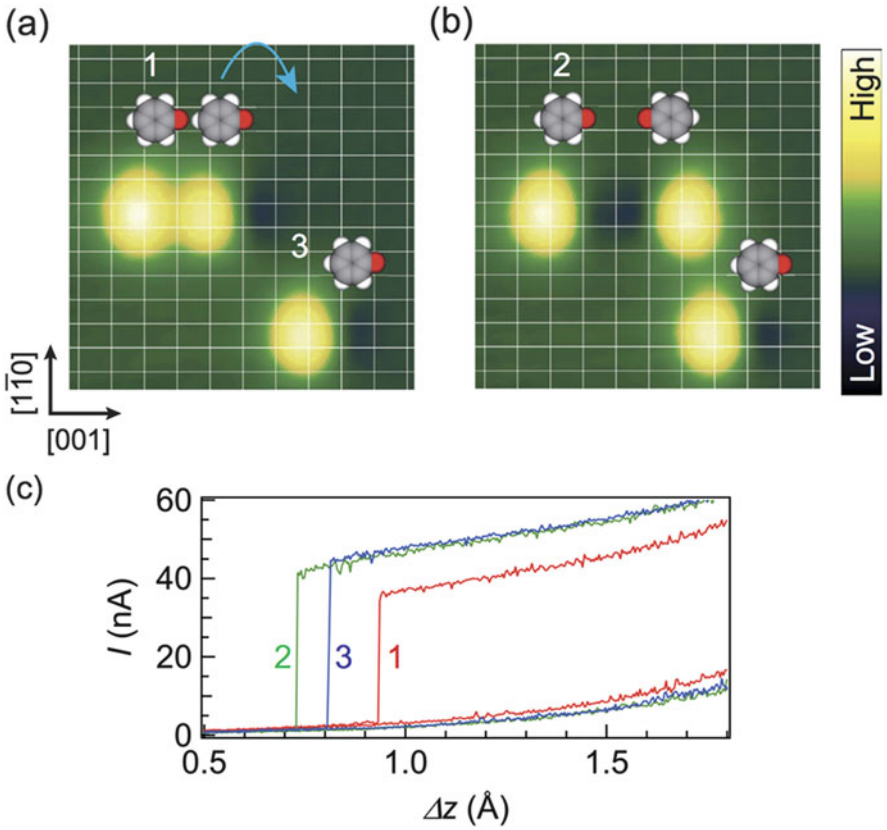

Fig. 2.20 STM images of phenoxy molecules on Cu(110) surface taken at 4.5 K before (**a**) and after (**b**) the flip of molecule next to the one denoted 1. (**c**) Current transient observed during approaching the STM tip to the molecules denoted *1*, *3*(*a*), and *2*(*c*) at the center position of each molecule. The *curves* not indicated by numbers are current transient taken at clean Cu(110) surface with the same STM tip used to form molecule junctions. Δz is displacement of the tip normal to the surface plane from the feedback point. Positive values correspond to the direction approaching to the surface [70]

adsorbed on a surface. And then, the surface is heated to cause chemical reactions between molecular units. Figure 2.21a shows an example of the molecular unit, dibromoterfluorene (DBTF), for the on-surface polymerization [75]. Figure 2.21b and c shows an experimental and calculated STM image of the DBTF molecule on an Au(111) surface at 10 K. Three intense lobes corresponding to the dimethyl groups connecting two phenyl rings in the DBTF molecule are imaged. When the Au(111) surface is heated, Br atoms dissociate from the molecule and C-C bond is formed between the molecules which thermally diffuse and collapse. Figure 2.21d, e shows STM images after heating the Au(111) surface at 520 K for 5 min. It is evident from the image that the long well-defined fluorene oligomer more than 100 nm is synthesized on the surface. The electrical conductance of the oligomer can be

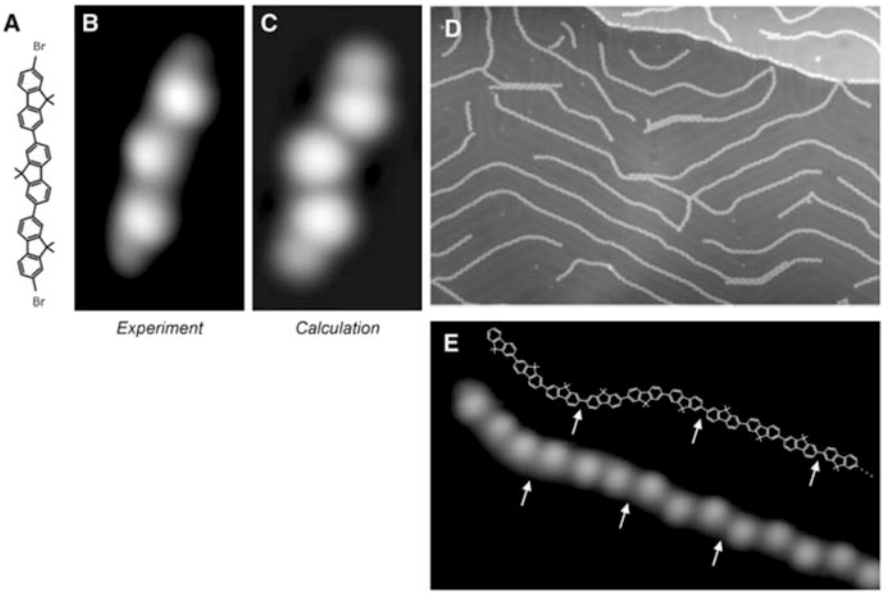

Fig. 2.21 Chemical structure (**a**) and observed (**b**) and calculated (**c**) STM images of DBTF. (**d**) STM image of gold surface after on-surface polymerization. (**e**) Magnified STM image for a polyfluorene oligomer and its molecular structure [75]

measured by contacting the STM tip with one end of the oligomer and lifting the molecule.

The on-surface polymerization is useful not only for preparation of samples for STM measurements but also for synthesizing molecules that are not prepared in solutions. In fact, the long fluorene polymer shown in Fig. 2.21d cannot be prepared in solutions due to the lack of solubility.

2.4 Summary and Perspective

In this chapter, three representative methods used to measure electrical properties of single-molecule junctions are explained. The major difficulty of measuring single-molecule junction is confirmation of single-molecule junctions and low yield of formation of the junction. The STM-BJ and MCBJ techniques solve these problems by using mobile electrodes and have become the standard methods. Conductance traces observed during the breaking of the metal wire by mechanical motion of the electrode enable researchers to detect the formation of single-molecule junctions and also repeat measurements for many times sufficient for statistical analysis. The STM-BJ is suitable for the statistical determination of the molecular conductance because the STM setup affords thousands of measurements contentiously. Even

simple statistical analysis using conductance histogram reveals interesting nature of the single-molecule junctions such as relation between conductance and contact geometries. More sophisticated analysis such as correlation analysis and conditional histogram would provide information to understand formation process of single-molecule junctions with different configurations. The MCBJ method is capable of sustaining a single-molecule junction for a long time enough to measure current-voltage characteristics and apply more sophisticated measurement methods introduced in Chap. 3.

External modulations such as electrostatic fields and magnetic fields of single-molecule junctions are still challenging. For this purpose, the MCBJ method encounters difficulties, although some challenges have been done. Different techniques such as electromigration are used. However, the capability of distance modulation is essential to confirm the formation of single-molecule junctions, and the method to measure external modulation with MCBJ should be developed.

The stability and imaging capability of UHV-LT-STM allows researchers not only to confirm the existence of a molecule and bonding site on a substrate but also to identify orientation of molecule that is essential for the study of molecular diodes. The electromechanical properties should be also investigated more precisely by using UHV-LT-AFM. Although it still is difficult to put large molecules on surfaces without contaminations, on-surface polymerization opens a new path to prepare large molecules on clean surfaces in vacuum.

The statistical approach to determine the conductance of a single molecule by the BJ method is reliable and successful. However, the deviation of the conductance histogram often reaches several orders of magnitude. Although this deviation can be justified because conductance values for a wide variety of structures are involved in the conductance histogram, it is not straightforward to understand what the peak value and width of the histogram represent. It can represent the most frequently observed plateau and/or the most long-lasting plateau in conductance transient curves. This difference can be problematic especially in low-temperature MCBJ measurements of long molecules because various metastable structures can be stably sustained. Other analytical method should be applied to understand the meaning of plagues in the conductance transient and peak of the conductance histogram as discussed in Chap. 3. Design of molecule junctions showing small conductance deviations should be developed for creating single-molecule devices. For this purpose, new anchor structures such as tripods [77, 78] and insulation of conductive path in a molecule should be studied such as discussed in Chaps. 5 and 6.

Fabrication of stable solid-state single-molecule devices is the most challenging topic remained. For this purpose, well-defined electrodes in atomic scale and robust contacts between electrodes and molecules are required. These requirements can be potentially fulfilled by using graphene and nanoribbons as electrodes [79]. Devices possessing functions of single molecules would be also produced by using self-assembled monolayers [80, 81].

References

1. Ashwell GJ, Sambles JR, Martin AS, Parker WG, Szablewski M (1990) Rectifying characteristics of Mg|($C_{16}H_{33}$-Q3CNQ LB film)|Pt structures. J Chem Soc Chem Commun 19:1374. http://doi.org/10.1039/c39900001374
2. Wang W, Lee T, Reed MA (2004) Elastic and inelastic electron tunneling in alkane self-assembled monolayers. J Phys Chem B 108(48):18398–18407. http://doi.org/10.1021/jp048904k
3. Cui XD (2001) Reproducible measurement of single-molecule conductivity. Science 294(5542):571–574. http://doi.org/10.1126/science.1064354
4. Dadosh T, Gordin Y, Krahne R, Khivrich I, Mahalu D, Frydman V, Bar-joseph I (2005) Measurement of the conductance of single conjugated molecules. Nature 436:2–6. http://doi.org/10.1038/nature03898
5. Jafri SHM, Löfås H, Blom T, Wallner A, Grigoriev A, Ahuja R, Leifer K (2015) Nanofabrication of molecular electronic junctions by targeted modification of metal-molecule bonds. Sci Rep 5:14431. http://doi.org/10.1038/srep14431
6. Kushmerick JG, Holt DB, Yang JC, Naciri J, Moore MH, Shashidhar R (2002) Metal-molecule contacts and charge transport across monomolecular layers: measurement and theory. Phys Rev Lett 89(8):086802. http://doi.org/10.1103/PhysRevLett.89.086802
7. Schwarz F, Lörtscher E (2014) Break-junctions for investigating transport at the molecular scale. J Phys Condens Matter 26(47):474201. http://doi.org/10.1088/0953-8984/26/47/474201
8. Xiang D, Jeong H, Lee T, Mayer D (2013) Mechanically controllable break junctions for molecular electronics. Adv Mater 25(35):4845–4867. http://doi.org/10.1002/adma.201301589
9. Tsutsui M, Taniguchi M (2012) Single molecule electronics and devices. Sensors (Basel, Switzerland) 12(6):7259–7298. http://doi.org/10.3390/s120607259
10. Van Ruitenbeek J, Scheer E, Weber HB (2005) Contacting individual molecules using mechanically controllable break junctions. Lect Notes Phys 680:253
11. Selzer Y, Allara DL (2006) Single-molecule electrical junctions. Annu Rev Phys Chem 57(1):593–623. http://doi.org/10.1146/annurev.physchem.57.032905.104709
12. Tao NJ (2006) Electron transport in molecular junctions. Nat Nanotechnol 1(3):173–181. http://doi.org/10.1038/nnano.2006.130
13. McCreery RL (2004) Molecular electronic junctions. Chem Mater 16(23):4477–4496. http://doi.org/10.1021/cm049517q
14. Metzger RM (2015) Unimolecular electronics. Chem Rev 115(11):5056–5115. http://doi.org/10.1021/cr500459d
15. Xu B (2003) Measurement of single-molecule resistance by repeated formation of molecular junctions. Science 301(5637):1221–1223. http://doi.org/10.1126/science.1087481
16. Reed MA (1997) Conductance of a molecular junction. Science 278(5336):252–254. http://doi.org/10.1126/science.278.5336.252
17. Li X, He J, Hihath J, Xu B, Lindsay SM, Tao N (2006) Conductance of single alkanedithiols: conduction mechanism and effect of molecule−electrode contacts. J Am Chem Soc 128(6):2135–2141. http://doi.org/10.1021/ja057316x
18. Ishtzuka K, Suzuki M, Fujii S, Takayama Y, Sato F, Fujihira M (2006) Effect of molecule-electrode contacts on single-molecule conductivity of π-conjugated system measured by scanning tunneling microscopy under ultrahigh vacuum. Jpn J Appl Phys Part 1 45(3 B):2037–2040. http://doi.org/10.1143/JJAP.45.2037
19. Li C, Pobelov I, Wandlowski T, Bagrets A, Arnold A, Evers F (2008) Charge transport in single Au|Alkanedithiol|Au junctions: coordination geometries and conformational degrees of freedom. J Am Chem Soc 130(17):19. http://doi.org/10.1021/ja0762386
20. He J, Chen F, Li J, Sankey OF, Terazono Y, Herrero C, Lindsay SM (2005) Electronic decay constant of carotenoid polyenes from single-molecule measurements. J Am Chem Soc 127(5):1384–1385. http://doi.org/10.1021/ja043279i

21. Yamada R, Kumazawa H, Noutoshi T, Tanaka S, Tada H (2008) Electrical conductance of oligothiophene molecular wires. Nano Lett 8(4):1237–1240. http://doi.org/10.1021/nl0732023
22. Venkataraman L, Klare JE, Nuckolls C, Hybertsen MS, Steigerwald ML (2006) Dependence of single-molecule junction conductance on molecular conformation. Nature 442(7105):904–907. http://doi.org/10.1038/nature05037
23. Chen F, Li X, Hihath J, Huang Z, Tao N (2006) Effect of anchoring groups on single-molecule conductance: comparative study of thiol-, amine-, and carboxylic-acid-terminated molecules. J Am Chem Soc 128(49):15874–15881. http://doi.org/10.1021/ja065864k
24. Park YS, Whalley AC, Kamenetska M, Steigerwald ML, Hybertsen MS, Nuckolls C, Venkataraman L (2007) Contact chemistry and single-molecule conductance: a comparison of phosphines, methyl sulfides, and amines. J Am Chem Soc 129(51):15768–15769. http://doi.org/10.1021/ja0773857
25. Venkataraman L, Park YS, Whalley AC, Nuckolls C, Hybertsen MS, Steigerwald ML (2007) Electronics and chemistry: varying single-molecule junction conductance using chemical substituents. Nano Lett 7(2):502–506. http://doi.org/10.1021/nl062923j
26. Troisi A, Ratner MA (2006) Molecular signatures in the transport properties of molecular wire junctions: what makes a junction "molecular"? Small 2(2):172–181. http://doi.org/10.1002/smll.200500201
27. Luo L, Choi SH, Frisbie CD (2011) Probing hopping conduction in conjugated molecular wires connected to metal electrodes. Chem Mater 23(3):631–645. http://doi.org/10.1021/cm102402t
28. Poot M, Osorio E, O'Neill K, Thijssen JM, Vanmaekelbergh D, van Walree CA, van der Zant HSJ (2006) Temperature dependence of three-terminal molecular junctions with sulfur end-functionalized tercyclohexylidenes. Nano Lett 6(5):1031–1035. http://doi.org/10.1021/nl0604513
29. Yamada R, Kumazawa H, Tanaka S, Tada H (2009) Electrical resistance of long oligothiophene molecules. Appl Phys Express 2(2). http://doi.org/10.1143/APEX.2.025002
30. Lee SK, Yamada R, Tanaka S, Chang GS, Asai Y, Tada H (2012) Universal temperature crossover behavior of electrical conductance in a single oligothiophene molecular wire. ACS Nano 6(6):5078–5082. http://doi.org/10.1021/nn3006976
31. Vrouwe S, van der Giessen E, van der Molen S, Dulic D, Trouwborst M, van Wees B (2005) Mechanics of lithographically defined break junctions. Phys Rev B 71(3):1–7. http://doi.org/10.1103/PhysRevB.71.035313
32. Zhou C, Muller CJ, Deshpande MR, Sleight JW, Reed M a (1995) Microfabrication of a mechanically controllable break junction in silicon. Appl Phys Lett 67(8):1160. http://doi.org/10.1063/1.114994
33. Perrin ML, Frisenda R, Koole M, Seldenthuis JS, Gil JA, Valkenier H, van der Zant HSJ (2014) Large negative differential conductance in single-molecule break junctions. Nat Nanotechnol 9(10):830–834. http://doi.org/10.1038/nnano.2014.177
34. Egle S, Bacca C, Pernau HF, Huefner M, Hinzke D, Nowak U, Scheer E (2010) Magnetoresistance of atomic-size contacts realized with mechanically controllable break junctions. Phys Rev B - Condens Matter Mater Phys 81(13):1–11. http://doi.org/10.1103/PhysRevB.81.134402
35. Jammalamadaka SN, Kuntz S, Berg O, Kittler W, Kannan UM, Chelvane JA, Sürgers C (2015) Remote control of magnetostriction-based nanocontacts at room temperature. Sci Rep 5:13621. http://doi.org/10.1038/srep13621
36. Yamada R, Noguchi M, Tada H (2011) Magnetoresistance of single molecular junctions measured by a mechanically controllable break junction method. Appl Phys Lett 98(5). http://doi.org/10.1063/1.3549190
37. Martin CA, Ding D, Sørensen JK, Bjørnholm T, van Ruitenbeek JM, van der Zant HSJ (2008) Fullerene-based anchoring groups for molecular electronics. J Am Chem Soc 130(40):13198–13199. http://doi.org/10.1021/ja804699a
38. Quek SY, Kamenetska M, Steigerwald ML, Choi HJ, Louie SG, Hybertsen MS, Venkataraman L (2009) Mechanically controlled binary conductance switching of a single-molecule junction. Nat Nanotechnol 4(4):230–234. http://doi.org/10.1038/nnano.2009.10

39. Wawrzyniak M, Martinek J, Susla B, Ilnicki G (2009) Correlation histograms in conductance measurements of nanowires formed at semiconductor interfaces. Acta Phys Pol A 115(1):384–386
40. Makk P, Tomaszewski D, Martinek J, Balogh Z, Csonka S, Wawrzyniak M, Halbritter A (2012) Correlation analysis of atomic and single-molecule junction conductance. ACS Nano 6(4):3411–3423. http://doi.org/10.1021/nn300440f
41. Mishchenko A, Zotti LA, Vonlanthen D, Bürkle M, Pauly F, Cuevas JC, Wandlowski T (2011) Single-molecule junctions based on nitrile-terminated biphenyls: a promising new anchoring group. J Am Chem Soc 133(2):184–187. http://doi.org/10.1021/ja107340t
42. Xia JL, Diez-Perez I, Tao NJ (2008) Electron transport in single molecules measured by a distance-modulation assisted break junction method. Nano Lett 8(7):1960–1964. http://doi.org/10.1021/nl080857a
43. Binnig G, Rohrer H, Gerber C, Weibel E (1982) Tunneling through a controllable vacuum gap. Appl Phys Lett 40(2):178–180. http://doi.org/10.1063/1.92999
44. Bruot C, Palma JL, Xiang L, Mujica V, Ratner MA, Tao N (2015) Piezoresistivity in single DNA molecules. Nat Commun 6(May):8032. http://doi.org/10.1038/ncomms9032
45. Díez-Pérez I, Hihath J, Lee Y, Yu L, Adamska L, Kozhushner MA, Tao N (2009) Rectification and stability of a single molecular diode with controlled orientation. Nat Chem 1(8):635–641. http://doi.org/10.1038/nchem.392
46. Diez-Perez I, Hihath J, Hines T, Wang Z-S, Zhou G, Müllen K, Tao N (2011) Controlling single-molecule conductance through lateral coupling of π orbitals. Nat Nanotechnol 6(4):226–231. http://doi.org/10.1038/nnano.2011.20
47. Xu B, Xiao X, Tao NJ (2003) Measurements of single-molecule electromechanical properties. J Am Chem Soc 125(52):16164–16165. http://doi.org/10.1021/ja038949j
48. Xu BQ, Li XL, Xiao XY, Sakaguchi H, Tao NJ (2005) Electromechanical and conductance switching properties of single oligothiophene molecules. Nano Lett 5(7):1491–1495. http://doi.org/10.1021/nl050860j
49. Frei M, Aradhya SV, Koentopp M, Hybertsen MS, Venkataraman L (2011) Mechanics and chemistry: single molecule bond rupture forces correlate with molecular backbone structure. Nano Lett 11(4):1518–1523. http://doi.org/10.1021/nl1042903
50. Aradhya SV, Frei M, Hybertsen MS, Venkataraman L (2012) Van der Waals interactions at metal/organic interfaces at the single-molecule level. Nat Mater 11(10):872–876. http://doi.org/10.1038/nmat3403
51. Yoshida K, Pobelov IV, Manrique DZ, Pope T, Mészáros G, Gulcur M, Wandlowski T (2015) Correlation of breaking forces, conductances and geometries of molecular junctions. Sci Rep 5:9002. http://doi.org/10.1038/srep09002
52. Perrin ML, Burzurí E, van der Zant HSJ (2015) Single-molecule transistors. Chem Soc Rev 44(4):902–919. http://doi.org/10.1039/C4CS00231H
53. Cui A, Dong H, Hu W (2015) Nanogap electrodes towards solid state single-molecule transistors. Small 11(46):6115–6141. http://doi.org/10.1002/smll.201501283
54. Kubatkin S, Danilov A, Hjort M, Cornil J, Brédas J-L, Stuhr-Hansen N, Bjørnholm T (2003) Single-electron transistor of a single organic molecule with access to several redox states. Nature 425(6959):698–701. http://doi.org/10.1038/nature02010
55. Martin CA, Smit RHM, van der Zant HSJ, van Ruitenbeek JM (2009) A nanoelectromechanical single-atom switch. Nano Lett 9(8):2940–2945. http://doi.org/10.1021/nl901355y
56. Xiang D, Jeong H, Kim D, Lee T, Cheng Y, Wang Q, Mayer D (2013) Three-terminal single-molecule junctions formed by mechanically controllable break junctions with side gating. Nano Lett 13(6):2809–2813. http://doi.org/10.1021/nl401067x
57. Martin CA, van Ruitenbeek JM, van der Zant HSJ (2010) Sandwich-type gated mechanical break junctions. Nanotechnology 21(26):265201. http://doi.org/10.1088/0957-4484/21/26/265201
58. Perrin ML, Verzijl CJO, Martin CA, Shaikh AJ, Eelkema R, Van Esch JH, Dulić D (2013) Large tunable image-charge effects in single-molecule junctions. Nat Nanotechnol 8(4):282–287. http://doi.org/10.1038/nnano.2013.26

59. Huang C, Rudnev AV, Hong W, Wandlowski T (2015) Break junction under electrochemical gating: testbed for single-molecule electronics. Chem Soc Rev 44:889–901. http://doi.org/10.1039/C4CS00242C
60. Li X, Hihath J, Chen F, Masuda T, Zang L, Tao N (2007) Thermally activated electron transport in single redox molecules. J Am Chem Soc 129(37):11535–11542. http://doi.org/10.1021/ja072990v
61. Lloyd JR (1997) Electromigration in thin film conductors. Defect Diffus Forum 143–147:1661–1672. http://doi.org/10.4028/www.scientific.net/DDF.143-147.1661
62. Strachan DR, Smith DE, Johnston DE, Park T-H, Therien MJ, Bonnell D a, Johnson AT (2005) Controlled fabrication of nanogaps in ambient environment for molecular electronics. Appl Phys Lett 86(4):043109. http://doi.org/10.1063/1.1857095
63. O'Neill K, Osorio EA, Van Der Zant HSJ (2007) Self-breaking in planar few-atom au constrictions for nanometer-spaced electrodes. Appl Phys Lett 90(13). http://doi.org/10.1063/1.2716989
64. Tsutsui M, Taniguchi M, Kawai T (2008) Fabrication of 0.5 nm electrode gaps using self-breaking technique. Appl Phys Lett 93(16):1–4. http://doi.org/10.1063/1.3006063
65. Houck AA, Labaziewicz J, Chan EK, Folk JA, Chuang IL (2005) Kondo effect in electromigrated gold break junctions. Nano Lett 5(9):1685–1688. http://doi.org/10.1021/nl050799i
66. Song H, Kim Y, Jang YH, Jeong H, Reed MA, Lee T (2009) Observation of molecular orbital gating. Nature 462(7276):1039–1043. http://doi.org/10.1038/nature08639
67. Suga H, Sumiya T, Furuta S, Ueki R, Miyazawa Y, Nishijima T, Naitoh Y (2012) Single-crystalline nanogap electrodes: enhancing the nanowire-breakdown process with a gaseous environment. ACS Appl Mater Interfaces 4(10):5542–5546. http://doi.org/10.1021/am301441a
68. Tsutsui M, Rahong S, Iizumi Y, Okazaki T, Taniguchi M, Kawai T (2011) Single-molecule sensing electrode embedded in-plane nanopore. Sci Rep 1:46. http://doi.org/10.1038/srep00046
69. Chen CJ (1993) Introduction to scanning tunneling microscopy. Oxford University Press, New York
70. Kitaguchi Y, Habuka S, Okuyama H, Hatta S, Aruga T, Frederiksen T, Ueba H (2015) Controlling single-molecule junction conductance by molecular interactions. Sci Rep 5:11796. http://doi.org/10.1038/srep11796
71. Tanaka H, Kawai T (1997) Scanning tunneling microscopy imaging and manipulation of DNA oligomer adsorbed on Cu(111) surfaces by a pulse injection method. J Vac Sci Technol B 15(3):602. http://doi.org/10.1116/1.589299
72. Yokoyama T, Kogure Y, Kawasaki M, Tanaka S, Aoshima K (2013) Scanning tunneling microscopy imaging of long oligothiophene wires deposited on Au(111) using electrospray ionization. J Phys Chem C 117(36):18484–18487. http://doi.org/10.1021/jp405411f
73. Rinke G, Rauschenbach S, Schrettl S, Hoheisel TN, Blohm J, Gutzler R, Kern K (2014) Soft-landing electrospray ion beam deposition of sensitive oligoynes on surfaces in vacuum. Int J Mass Spectrom 377:228–234. http://doi.org/10.1016/j.ijms.2014.06.026
74. Grill L, Dyer M, Lafferentz L, Persson M, Peters MV, Hecht S (2007) Nano-architectures by covalent assembly of molecular building blocks. Nat Nanotechnol 2(11):687–691. http://doi.org/10.1038/nnano.2007.346
75. Lafferentz L, Ample F, Yu HB, Hecht S, Joachim C, Grill L (2009) Conductance of a single conjugated polymer as a continuous function of its length. Science 323(5918):1193–1197. http://doi.org/10.1126/science.1168255
76. Nacci C, Ample F, Bleger D, Hecht S, Joachim C, Grill L (2015) Conductance of a single flexible molecular wire composed of alternating donor and acceptor units. Nat Commun 6:7397. http://doi.org/10.1038/ncomms8397
77. Ie Y, Hirose T, Nakamura H, Kiguchi M, Takagi N, Kawai M, Aso Y (2011) Nature of electron transport by pyridine-based tripodal anchors: potential for robust and conductive single-molecule junctions with gold electrodes. J Am Chem Soc 133(9):3014–3022. http://doi.org/10.1021/ja109577f

78. Ie Y, Tanaka K, Tashiro A, Lee SK, Testai HR, Yamada R, Aso Y (2015) Thiophene-based tripodal anchor units for hole transport in single-molecule junctions with gold electrodes. J Phys Chem Lett 6(18):3754–3759. http://doi.org/10.1021/acs.jpclett.5b01662
79. Ullmann K, Coto PB, Leitherer S, Molina-Ontoria A, Martin N, Thoss M, Weber HB (2015) Single-molecule junctions with epitaxial graphene nanoelectrodes. Nano Lett 15(5):3512–3518. http://doi.org/10.1021/acs.nanolett.5b00877
80. Ru J, Szeto B, Bonifas A, McCreery RL (2010) Microfabrication and integration of diazonium-based aromatic molecular junctions. ACS Appl Mater Interfaces 2(12):3693–3701. http://doi.org/10.1021/am100833e
81. Seo S, Min M, Lee SM, Lee H (2013) Photo-switchable molecular monolayer anchored between highly transparent and flexible graphene electrodes. Nat Commun 4(May):1920. http://doi.org/10.1038/ncomms2937